

Spherical Mixture Integration for Latent Embedding Alignment across Multi-Source Feature Spaces

Yuming Zhang^{1*}, Congyuan Duan^{2*}, Dong Xia², Doudou Zhou^{3†}, Tianxi Cai^{1†}

¹Department of Biostatistics, Harvard T.H. Chan School of Public Health

²Department of Mathematics, Hong Kong University of Science and Technology

³Department of Statistics and Data Science, National University of Singapore

Abstract

Multi-institutional electronic health record (Multi-EHR) data have emerged as a powerful resource for developing predictive models to support clinical decisions and for generating reliable real-world evidence. By aggregating information from diverse patient populations and institutions, they enhance the robustness and generalizability of models and findings. However, analyzing multi-EHR remains challenging because disparate institutions rarely map all data elements to common ontology, and raw EHR codes are often overly granular and institution-specific, fragmenting representations of the same clinical concept. Hence, integrative analysis must overcome two key hurdles: harmonizing codes with the same clinical meaning (synonymy), and aligning institutional feature spaces. To address these challenges, we propose SMILE, a Spherical Mixture Integration for Latent Embedding alignment across multi-source feature spaces, where embeddings from heterogeneous sources serve as privacy-preserving summaries of clinical concepts and sparse auxiliary relationship pairs provide weak supervision on the latent geometry. Synonymy is modeled via a mixture of von Mises-Fisher distributions, yielding unified representations that consolidate semantically equivalent raw codes. We develop a composite quasi-likelihood estimation procedure and establish non-asymptotic error bounds for latent representations and mixture mean directions, together with consistent recovery of synonym clusters. The theory quantifies statistical gains from integrating multiple sources and auxiliary knowledge graph information. Simulations and a multi-institutional EHR application demonstrate improved alignment and synonym clustering.

Keywords: Electronic Health Records; Multi-source Learning; Spherical Mixture Models; Representation Learning.

*Zhang and Duan contributed equally to this work.

†Zhou and Cai contributed equally as corresponding authors. Emails: ddzhou@nus.edu.sg, tcgai@hsph.harvard.edu.

1 Introduction

1.1 Background

Multi-institutional electronic health record (EHR) data offers great opportunities for advancing predictive modeling to support clinical decisions and generating high-quality real-world evidence (Marwaha et al., 2024). Jointly analyzing data across health systems enables analyses at greater scale, captures broader clinical heterogeneity, and supports findings that generalize more reliably across patient populations and care settings (Bianchi et al., 2024; Sittig et al., 2012). Such diversity is critical for improving model transportability and mitigating site-specific bias.

Realizing this promise, however, requires overcoming significant integration challenges. Health systems often use different coding standards, local documentation practices, and incomplete mappings to shared ontologies (Garcia et al., 2025). Although standardized ontologies such as ICD-9 (Brämer, 1988), RxNorm (Liu et al., 2005), and Logical Observation Identifiers Names and Codes (LOINC) (McDonald et al., 2003) provide shared vocabularies, local EHR codes are often only partially mapped to these standards (Gan et al., 2025; Hong et al., 2021). Moreover, many raw EHR codes are highly granular, leading to fragmented and sparse representations of clinically similar concepts. Consequently, each institution induces its own high-dimensional feature space, and the union of these spaces across sites is heterogeneous, partially overlapping, and mis-aligned. Effective cross-site modeling therefore requires both consolidating semantically equivalent or closely related codes into coherent concept groupings and aligning heterogeneous institutional feature spaces.

Importantly, this challenge extends beyond missing data to representation-level incompatibility. Restricting analyses to features shared across sites discards valuable information, while ad hoc aggregation of unmatched codes risks introducing measurement error and distorting cross-site comparisons. Models trained on naively pooled features may also fail

to generalize when clinically equivalent codes are encoded differently. These limitations motivate methods that operate directly on learned representations rather than raw codes (Si et al., 2021; Choi et al., 2016; Zhou et al., 2026).

From a statistical perspective, such multi-institutional integration can be formulated as a coupled latent variable problem. Across institutions and data modalities, observed features constitute a noisy and partially overlapping view of a shared but unobserved set of underlying clinical concepts. The inferential goals are to recover a common latent representation from these heterogeneous and incomplete views, and to identify sets of synonymous features corresponding to the same underlying concept in the absence of fully observed correspondences. Feature-space misalignment obscures latent synonymy, while failure to resolve synonymy artificially inflates dimensionality and further complicates alignment. These inter-dependencies necessitate a unified framework that jointly addresses representation alignment and latent concept recovery under partial overlap.

In practice, direct sharing of patient-level data across institutions is often infeasible due to privacy, regulatory, and governance constraints. To enable integrative analyses under these restrictions, institutions instead construct privacy-preserving summary representations of their local data that can be shared to support federated or distributed learning without exposing individual-level records (Li et al., 2023; Brat et al., 2020). For feature alignment in particular, sites may share summary statistics that characterize feature distributions, such as co-occurrence-based measures or embedding-derived representations, to facilitate cross-institutional integration (Hong et al., 2021; Li et al., 2024; Zhou et al., 2026). These summaries retain substantial structural information about relationships among features while avoiding direct patient-level data transfer. Accordingly, we model the observed embeddings as heterogeneous and noisy realizations of a latent geometric structure shared across institutions. The resulting statistical objective is to recover this common latent geometry together with the grouping structure induced by concept-level synonymy.

In this work, we develop **Spherical Mixture Integration for Latent Embeddings** (SMILE) alignment, a probabilistic framework that jointly addresses representation alignment and synonym recovery across multi-source feature spaces. SMILE integrates a multi-source latent factor model, which projects heterogeneous institutional views into a shared low-dimensional space, with a spherical mixture component that captures latent synonym groups as concentrated mean directions on the unit sphere. Auxiliary relational information from existing knowledge graph is incorporated through likelihood-based components that propagate weak supervision across the latent geometry. By coupling alignment and clustering within a single generative framework, SMILE enables coherent recovery of harmonized representations and underlying clinical concepts rather than treating these tasks as separate sequential steps.

1.2 Related Works

Our work is related to the multi-view integration literature, which decomposes variation into shared and view-specific components under the assumption that all views are measured on a common, aligned feature set. Representative examples include JIVE, AJIVE, and related structured factor models for multi-block data (Lock et al., 2013; Feng et al., 2018; Zhou et al., 2015; Yang and Michailidis, 2016; Gaynanova and Li, 2019; Park and Lock, 2020; Lock et al., 2022; Yi et al., 2023). These methods yield principled low-rank summaries and interpretable shared-versus-specific structure, but their reliance on aligned coordinates limits their applicability to our setting where each source has its own vocabulary and overlap is only partial, leaving a methodological gap for integrating views with heterogeneous feature spaces.

When feature spaces differ across sources, alignment is often formulated as learning mappings into a common latent space using geometric, distributional, or weak correspondence constraints. This regime is studied broadly under heterogeneous transfer learning and re-

lated representation-alignment formulations (Day and Khoshgoftaar, 2017; Feuz and Cook, 2015; Bao et al., 2023). In multi-institutional EHR studies, a growing literature instantiates this idea by aligning code representations across sites using partially shared vocabularies, ontology anchors, or privacy-preserving summary representations (e.g., embeddings or aggregated co-occurrence statistics) that can be shared without releasing patient-level records (Hong et al., 2021; Zhou et al., 2022; Li et al., 2023; Brat et al., 2020; Li et al., 2024; Zhou et al., 2026). Closely related work on embedding-space alignment (e.g., cross-lingual word embeddings) shows that meaningful alignment can be achieved with limited supervision via approximately orthogonal transformations and self-learning, while emphasizing the structural assumptions needed for identifiability (Alaux et al., 2018; Grave et al., 2019).

In multi-EHR integration, partially overlapping feature spaces is further compounded by the fact that correspondences are not merely missing but often many-to-one, in that multiple local codes may refer to the same clinical concept. This turns alignment into a joint alignment-and-clustering problem, where the goal is to recover latent synonym groups while constructing a harmonized embedding space. Existing EHR pipelines typically address this synonymy via manual ontology mappings or heuristic code aggregation, which are often incomplete across institutions and decoupled from representation alignment. Directional mixture models, such as mixtures of von Mises-Fisher distributions, provide a natural probabilistic mechanism for representing tight semantic clusters on the unit sphere (Gopal and Yang, 2014; Barbaro and Rossi, 2021; Shi et al., 2021), offering a principled alternative to such ad hoc synonym handling. Nevertheless, these methods do not tackle the joint alignment-and-clustering problem. As a result, there is currently no unified framework that jointly pools synonym and alignment evidence within a single statistical objective, especially when only weak anchors are available.

Incorporating auxiliary relational information connects our framework to the literatures on community detection, stochastic block models (SBMs), and network models with side

information (Holland et al., 1983; Lei and Rinaldo, 2015; Hu and Wang, 2024; Pei et al., 2022). However, our setting departs fundamentally from classic SBM regimes. In synonym recovery, the number of latent clusters grows with the vocabulary size, while most clusters remain small and may even be finite. Moreover, we must simultaneously integrate multiple heterogeneous relation types and multi-view embeddings, rather than modeling a single homogeneous network. Although SBMs with a growing number of communities have been studied (Choi et al., 2012; Rohe et al., 2011), existing theory typically assumes community sizes also grow sufficiently fast and focuses on a single relation type. These assumptions do not cover the regime we consider, where the number of clusters diverges while cluster sizes remain small, and heterogeneous relational views must be jointly leveraged for many-to-one synonym clustering. As such, our work addresses a previously uncharacterized high-cluster-number, small-cluster-size, multi-view recovery problem that falls outside of the guarantees of existing network theory.

1.3 Contributions

We propose SMILE to address the lack of a unified framework for simultaneous alignment and synonym recovery in multi-source settings characterized by heterogeneous vocabularies, partial overlap, and many-to-one correspondences. Rather than separating embedding alignment and clustering into sequential steps, SMILE treats them as a single joint estimation problem. By modeling heterogeneous embeddings and auxiliary relations as complementary views of a shared latent geometry, SMILE integrates multi-source latent factor modeling with a spherical mixture component that directly encodes concept-level grouping. Auxiliary relational information enters through logistic components that provide weak supervision, allowing the model to leverage sparse and noisy similarity signals. Estimation via a composite likelihood framework accommodates heterogeneous embedding dimensions and partial correspondence while maintaining computational tractability.

From a theoretical standpoint, we provide the first recovery guarantees tailored to the high-cluster-number, small-cluster-size, multi-view regime common in real-world EHR data integration. We establish non-asymptotic error bounds for feature-level latent representations and cluster-level mean directions, along with consistency of synonym cluster recovery as vocabulary size grows. These results clarify how estimation accuracy scales with the number and quality of sources, the degree of vocabulary overlap, and the availability of auxiliary relational information. Empirically, we demonstrate that SMILE improves both multi-source feature alignment and synonym clustering relative to existing embedding-alignment and clustering baselines, in simulations and a real-world multi-institutional EHR application. Taken together, our results demonstrate that jointly harmonizing multiple sources, auxiliary relational information, and sparse correspondence signals can materially enhance multi-EHR integration and analysis.

2 The SMILE Methodology

2.1 Generative Model for Latent Geometry

Our goal is to project heterogeneous, partially overlapping high-dimensional embeddings into a shared low-dimensional space to recover latent synonym groups. Let $[n] \equiv \{1, \dots, n\}$ index distinct EHR features (both standard ontology and institution-specific codes). Embeddings are obtained from L heterogeneous sources. For each source $l \in [L]$, let $\mathcal{S}_l \subset [n]$ be the subset of features with embeddings from that source, with size $n_l \equiv |\mathcal{S}_l|$. We assume $\cup_{l=1}^L \mathcal{S}_l = [n]$, so every feature appears in at least one source, though overlaps may be partial. Define $N \equiv \sum_{l=1}^L n_l$ as the total number of feature instances across sources; the ratio N/n is the average number of source-level replicates per feature. For each feature $i \in \mathcal{S}_l$, let $\mathbf{U}_i^{(l)} \in \mathbb{R}^{r_l}$ be its unit-norm embedding from source l , where r_l may be large. In practice, these source-specific embeddings are typically learned from site-specific

co-occurrence patterns (Arora et al., 2015) or from pretrained language models (PLMs) applied to semantic code descriptions (e.g., Liu et al. 2020; Yuan et al. 2022). To achieve alignment and clustering, our framework SMILE specifies a joint generative model with four components: a multi-source factor model for the embeddings, a spherical mixture for synonym groups, and logistic models for auxiliary relational information, as detailed below.

First, we model the high-dimensional, source-specific embeddings using a multi-source latent factor model. Each feature i has a shared, unit-norm latent representation $\mathbf{V}_i \in \mathbb{R}^r$, where $r \ll r_l$ and $r \geq 2$. Conditional on $\{\mathbf{V}_i\}_{i \in [n]}$, the observed embeddings follow a multi-view latent factor model

$$\mathbf{U}_i^{(l)} = \mathbf{W}_l \mathbf{V}_i + \mathbf{E}_i^{(l)}, \quad i \in \mathcal{S}_l, \quad (1)$$

where $\mathbf{W}_l \in \mathbb{R}^{r_l \times r}$ is a source-specific loading matrix of rank r , and the noise vector $\mathbf{E}_i^{(l)}$ has independent mean-zero sub-Gaussian entries with variance σ^2 . Projection into this shared latent space reconciles the partially overlapping feature sets across sources, with $\{\mathbf{V}_i\}_{i \in [n]}$ identifiable only up to a global orthogonal transformation. For brevity, we henceforth write $\{\mathbf{V}\}$ for the collection of $\{\mathbf{V}_i\}_{i \in [n]}$.

Second, to recover the latent synonym groups, we assume that the shared representations $\{\mathbf{V}\}$ arise from a mixture of K von Mises-Fisher (vMF) distributions on the unit hypersphere:

$$\mathbf{V}_i \sim f_r(\mathbf{x}; \boldsymbol{\mu}_{z_i}, \kappa), \quad f_r(\mathbf{x}; \boldsymbol{\mu}, \kappa) = C_r(\kappa) \exp(\kappa \boldsymbol{\mu}^\top \mathbf{x}), \quad (2)$$

where $z_i \in [K]$ denotes the latent cluster membership (synonym group) of feature i , $\boldsymbol{\mu}_k$ is the unit-norm mean direction of cluster k , and $\kappa \geq 0$ is a common concentration parameter. The normalizing constant is given by $C_r(\kappa) = \kappa^{r/2-1} / \{(2\pi)^{r/2} I_{r/2-1}(\kappa)\}$, with $I_v(\cdot)$ denoting the modified Bessel function of the first kind at order v . By modeling each mean direction $\boldsymbol{\mu}_k$ as a concept-level embedding, this formulation allows synonymous features to realistically fluctuate around a shared center rather than collapsing to a single point, cap-

turing source-specific variation while preserving the geometric cohesion of the groups. In practice, the total number of clusters K can be selected in a data-driven manner, typically guided by auxiliary domain knowledge that provides partial cluster membership labels, such as existing medical ontologies in the specific case of EHR data.

Finally, we incorporate sparsely observed auxiliary knowledge graph information through two logistic models to supervise the latent geometry. To enforce broad concept-level coherence, the first model links similarity labels $\delta_{ij}^{(S)} \in \{0, 1\}$ (e.g., “Acetaminophen” and “Ibuprofen”) to the cluster means:

$$\mathbb{P}(\delta_{ij}^{(S)} = 1 | \boldsymbol{\mu}_{z_i}, \boldsymbol{\mu}_{z_j}, \beta_1, \beta_2) = \frac{\exp(\beta_1 + \beta_2 \boldsymbol{\mu}_{z_i}^\top \boldsymbol{\mu}_{z_j})}{1 + \exp(\beta_1 + \beta_2 \boldsymbol{\mu}_{z_i}^\top \boldsymbol{\mu}_{z_j})}, \quad (3)$$

where β_1 controls observation sparsity and β_2 dictates geometric alignment. To refine fine-grained, feature-level geometry, the second model links broader functional relatedness labels $\delta_{ij}^{(R)} \in \{0, 1\}$ (e.g., “Type 2 Diabetes” and “Metformin”) directly to the latent representations:

$$\mathbb{P}(\delta_{ij}^{(R)} = 1 | \mathbf{V}_i, \mathbf{V}_j, \beta_3, \mathbf{R}) = \frac{\exp(\beta_3 + \mathbf{V}_i^\top \mathbf{R} \mathbf{V}_j)}{1 + \exp(\beta_3 + \mathbf{V}_i^\top \mathbf{R} \mathbf{V}_j)}, \quad (4)$$

where β_3 controls observation density and the symmetric matrix \mathbf{R} weights the latent dimensions. Crucially, neither relation requires fully observed pairs across the feature space.

2.2 Composite Quasi-likelihood Estimation

To estimate the latent embeddings $\{\mathbf{V}\}$, concept-level means $\{\boldsymbol{\mu}\}$, and cluster labels $\{z\}$, we adopt a composite quasi-likelihood approach. Because the observed data combine multi-source embeddings with sparsely sampled relational pairs, a fully specified joint likelihood is neither natural nor necessary. Instead, we construct a unified, computationally tractable objective by summing the conditional (quasi-)likelihoods of the four model components (1)–(4), estimating all other parameters jointly as nuisance variables.

For the multi-source latent factor model (1), we enforce the geometric alignment of heterogeneous embeddings using a dimension-normalized squared loss

$$\ell_{\text{lr}}(\{\mathbf{V}\}, \{\mathbf{W}\}) = \frac{1}{N} \sum_{l=1}^L \sum_{i \in \mathcal{S}_l} \frac{1}{r_l} \left\| \mathbf{U}_i^{(l)} - \mathbf{W}_l \mathbf{V}_i \right\|_2^2. \quad (5)$$

For the vMF mixture (2), we enforce the concentration of latent embeddings around their concept-level mean directions by minimizing the negative log-likelihood:

$$\ell_{\text{vmf}}(\{\mathbf{V}\}, \{\boldsymbol{\mu}\}, \kappa) = -\frac{1}{nK} \sum_{i=1}^n \log \left\{ \sum_{k=1}^K f_r(\mathbf{V}_i; \boldsymbol{\mu}_k, \kappa) \pi_{ik} \right\}, \quad \text{with } \pi_{ik} \equiv \mathbb{P}(z_i = k). \quad (6)$$

Here, the prior probabilities $\{\pi_{ik}\}$ allow us to flexibly incorporate partial knowledge of cluster membership (e.g., from existing ontologies or feature-type constraints) as probabilistic guidance for synonym recovery, without imposing hard labels.

Finally, we formulate the negative log-likelihoods for the sparsely observed relational data based on their respective positive (\mathcal{P}_i) and negative (\mathcal{N}_i) sets, $\Omega_i^{(S)} \equiv \mathcal{P}_i^{(S)} \cup \mathcal{N}_i^{(S)}$ and $\Omega_i^{(R)} \equiv \mathcal{P}_i^{(R)} \cup \mathcal{N}_i^{(R)}$, with total observed pair counts denoted by n_S and n_R . The loss for similarity pairs (3) links annotations directly to concept-level geometry:

$$\ell_{\text{sim}}(\{\boldsymbol{\mu}\}, \beta_1, \beta_2) = -\frac{1}{n_S} \sum_{i=1}^n \sum_{j \in \Omega_i^{(S)}} \log \left\{ \sum_{k_1, k_2 \in [K]} \mathbb{P}(\delta_{ij}^{(S)} | \boldsymbol{\mu}_{k_1}, \boldsymbol{\mu}_{k_2}, \beta_1, \beta_2) \pi_{ik_1} \pi_{jk_2} \right\}, \quad (7)$$

and the loss for related pairs (4) informs the fine-scale latent geometry independently of cluster membership:

$$\ell_{\text{rel}}(\{\mathbf{V}\}, \beta_3, \mathbf{R}) = -\frac{1}{n_R} \sum_{i=1}^n \sum_{j \in \Omega_i^{(R)}} \log \mathbb{P}(\delta_{ij}^{(R)} | \mathbf{V}_i, \mathbf{V}_j, \beta_3, \mathbf{R}), \quad (8)$$

where $\mathbb{P}(\delta_{ij}^{(S)} | \boldsymbol{\mu}_{k_1}, \boldsymbol{\mu}_{k_2}, \beta_1, \beta_2)$ and $\mathbb{P}(\delta_{ij}^{(R)} | \mathbf{V}_i, \mathbf{V}_j, \beta_3, \mathbf{R})$ are the standard Bernoulli likelihoods derived from the logistic formulations in (3) and (4) respectively.

Bringing these components together, the composite estimator is defined as the minimizer of the weighted sum of the four losses:

$$\begin{aligned} \{\widehat{\mathbf{V}}\}, \{\widehat{\mathbf{W}}\}, \{\widehat{\boldsymbol{\mu}}\}, \widehat{\kappa}, \widehat{\beta}_1, \widehat{\beta}_2, \widehat{\beta}_3, \widehat{\mathbf{R}} \equiv \arg \min & \ell_{\text{lr}}(\{\mathbf{V}\}, \{\mathbf{W}\}) + w_{\text{vmf}} \ell_{\text{vmf}}(\{\mathbf{V}\}, \{\boldsymbol{\mu}\}, \kappa) + \\ & w_{\text{sim}} \ell_{\text{sim}}(\{\boldsymbol{\mu}\}, \beta_1, \beta_2) + w_{\text{rel}} \ell_{\text{rel}}(\{\mathbf{V}\}, \beta_3, \mathbf{R}), \end{aligned} \quad (9)$$

subject to the geometric constraints $\|\mathbf{V}_i\|_2 = 1$ for all i , $\|\boldsymbol{\mu}_k\|_2 = 1$ for all k , $\kappa \geq 0$, and symmetric \mathbf{R} . The weights $w_{\text{vmf}}, w_{\text{sim}}, w_{\text{rel}} \geq 0$ control the relative influence of each model component. Since each loss is normalized by its effective sample size, these weights primarily serve to balance heterogeneous noise levels and varying information content across the different data sources. In practice, they are selected in a data-driven manner and yield stable performance under moderate variations.

2.3 Algorithm

The composite objective (9) is solved using an alternating blockwise procedure outlined in Algorithm 1. We first initialize feature-level embeddings $\{\mathbf{V}\}$ by fitting only the multi-source latent factor and relatedness components, which avoids concept-level structure and thus does not require cluster labels or mean directions. We then initialize the concept-level parameters. The initialization for the mean directions $\{\boldsymbol{\mu}\}$ appears particularly crucial in practice, which, for example, can be obtained using spherical k -means on the initial embeddings. Because the synonym clusters are latent, we naturally employ an expectation-maximization (EM) algorithm to update the vMF mixture parameters and cluster assignments given current embeddings, and alternate this with refinement of the embeddings and feature-level parameters given the updated concept-level structure. Each blockwise update is implemented via gradient-based optimization under the relevant geometric constraints. Through iterations, the procedure leverages all available information (both the vMF mixture structure that encodes synonymy and the auxiliary relational pairs) within a single composite objective.

Algorithm 1 The SMILE algorithm

Input: Source-specific embeddings $\{\mathbf{U}\}$, relational pairs $\{\delta^{(s)}\}, \{\delta^{(R)}\}$, prior probabilities $\{\pi_{ik}\}$, weights $\{w_{\text{vmf}}, w_{\text{sim}}, w_{\text{rel}}\}$, initial values for all parameters.

Output: Estimates for $\{\mathbf{V}\}, \{\boldsymbol{\mu}\}, \{z\}$.

Step 1 (Initialization): Set $s = 1$. Initialize $\{\mathbf{V}\}$ by minimizing (9) with $w_{\text{vmf}} = w_{\text{sim}} = 0$, yielding $\{\widehat{\mathbf{V}}^{(s-1)}\}, \{\widehat{\mathbf{W}}^{(s-1)}\}, \widehat{\beta}_3^{(s-1)}, \widehat{\mathbf{R}}^{(s-1)}$. This step uses only feature-level alignment and relations, requiring no cluster labels or mean directions.

Step 2 (Concept-level update): Fixing $\{\widehat{\mathbf{V}}^{(s-1)}\}$, update $\{\boldsymbol{\mu}\}, \kappa, \beta_1, \beta_2, \{z\}$ by minimizing (9) with $w_{\text{rel}} = 0$ using an EM algorithm (see Supplement A for details), yielding $\{\widehat{\boldsymbol{\mu}}^{(s)}\}, \widehat{\kappa}^{(s)}, \widehat{\beta}_1^{(s)}, \widehat{\beta}_2^{(s)}, \{\widehat{z}^{(s)}\}$. This step updates concept-level geometry and cluster assignments given fixed feature-level embeddings.

Step 3 (Feature-level refinement): Fixing $\{\widehat{\boldsymbol{\mu}}^{(s)}\}, \widehat{\kappa}^{(s)}, \{\widehat{z}^{(s)}\}$, refine $\{\mathbf{V}\}, \{\mathbf{W}\}, \beta_3, \mathbf{R}$ by minimizing (9) with $w_{\text{sim}} = 0$, yielding $\{\widehat{\mathbf{V}}^{(s)}\}, \{\widehat{\mathbf{W}}^{(s)}\}, \widehat{\beta}_3^{(s)}, \widehat{\mathbf{R}}^{(s)}$. This step uses only terms involving feature-level variables.

Step 4 (Iteration): Set $s \leftarrow s + 1$ and repeat Steps 2–3 until convergence.

3 Theoretical Properties

This section establishes the identifiability of the SMILE model (Section 3.1) and provides theoretical guarantees for the SMILE estimator (Sections 3.2 and 3.3). Specifically, we focus on three theoretical results: (i) a non-asymptotic recovery bound for the latent embeddings $\{\mathbf{V}\}$, (ii) an analogous bound for the cluster mean directions $\{\boldsymbol{\mu}\}$, and (iii) consistency of the induced clustering $\{\widehat{z}\}$.

We introduce the necessary notations before proceeding. For a matrix \mathbf{A} , $\lambda_{\min}(\mathbf{A})$ and $\lambda_{\max}(\mathbf{A})$ denote its smallest and largest singular values. We write $\|\mathbf{A}\|$ for the operator (spectral) norm of \mathbf{A} and $\|\mathbf{A}\|_F$ for its Frobenius norm. For a vector \mathbf{a} , $\|\mathbf{a}\|_2$ denotes the Euclidean norm. Let $\mathbb{O}^{r \times r} \equiv \{\mathbf{O} \in \mathbb{R}^{r \times r} : \mathbf{O}^\top \mathbf{O} = \mathbf{I}_r\}$ be the orthogonal group. We write

$a \lesssim b$ and $b \gtrsim a$ if $a \leq Cb$ for some finite positive constant C , and $a \wedge b \equiv \min\{a, b\}$. The indicator function is denoted by $\mathbb{1}(\cdot)$.

3.1 Identifiability of the SMILE Model

The SMILE model is identifiable only up to two natural transformations of its latent parameters. For any orthogonal matrix $\mathbf{O} \in \mathbb{O}^{r \times r}$ and any permutation τ of $[K]$ preserving the prior probabilities $\{\pi_{ik}\}$ (i.e., $\pi_{i,\tau(k)} = \pi_{ik}$ for all $i \in [n], k \in [K]$), the simultaneous transformation

$$\mathbf{V}'_i = \mathbf{O}\mathbf{V}_i, \quad \boldsymbol{\mu}'_k = \mathbf{O}\boldsymbol{\mu}_{\tau(k)}, \quad z'_i = \tau^{-1}(z_i), \quad \mathbf{W}'_l = \mathbf{W}_l\mathbf{O}^\top, \quad \mathbf{R}' = \mathbf{O}\mathbf{R}\mathbf{O}^\top,$$

leaves the joint distribution of the observed quantities $\{\mathbf{U}\}, \{\delta^{(S)}\}, \{\delta^{(R)}\}$ unchanged. Indeed, the multi-view factor model in (1) depends only on $\mathbf{W}'_l\mathbf{V}'_i = \mathbf{W}_l\mathbf{V}_i$; the bilinear form in the relatedness logistic model in (4) satisfies $(\mathbf{V}'_i)^\top \mathbf{R}' \mathbf{V}'_j = \mathbf{V}_i^\top \mathbf{R} \mathbf{V}_j$; the similarity logistic model in (3) relies only on $\boldsymbol{\mu}_{z'_i}^\top \boldsymbol{\mu}_{z'_j}$, which is invariant under simultaneous rotation of $\{\boldsymbol{\mu}_k\}$ together with the relabeling $z'_i = \tau^{-1}(z_i)$; and the prior $\pi_{i,z'_i} = \pi_{i,\tau^{-1}(z_i)} = \pi_{i,z_i}$ since τ preserves the prior probabilities $\{\pi_{ik}\}$.

Therefore, the SMILE model is identifiable only up to (i) a common orthogonal rotation $\mathbf{O} \in \mathbb{O}^{r \times r}$ in the latent space, and (ii) a permutation τ of cluster labels preserving the prior probabilities $\{\pi_{ik}\}$. Throughout this section, the notations $\mathbf{V}_i, \boldsymbol{\mu}_k, z_i, \mathbf{W}_l, \mathbf{R}$ denote the true values of these parameters, at a single fixed representative of this equivalence class; the orthogonal matrix \mathbf{O} and permutation τ that appear in the theorem statements below act as the alignment between this fixed representative and the SMILE estimator (numerically, the algorithm's output whose coordinate frame is set by the non-convex optimization).

3.2 Assumptions

The analysis below follows the well-initialized non-convex M -estimator framework popularized by Balakrishnan et al. (2017) for the EM algorithm and Loh and Wainwright (2015) for regularized M -estimators with non-convex loss; see also Wang et al. (2015); Ma et al. (2020) for related results in high-dimensional EM and matrix factorization. Two ingredients enable the analysis: (i) Algorithm 1 is initialized at parameters lying in a neighborhood of the truth (Definition 1), provided in practice by a matrix-factorization-based initialization for $\{\mathbf{V}\}$ and a clustering-based initialization for $\{\boldsymbol{\mu}\}$ (e.g., k -means on the initial $\{\mathbf{V}\}$); and (ii) the composite loss is well-behaved on this neighborhood under regularity conditions.

Definition 1 (Neighborhood of the truth). *We say that the parameter values $\{\mathbf{V}'\}$, $\{\boldsymbol{\mu}'\}$, $\beta'_1, \beta'_2, \beta'_3, \mathbf{R}', \kappa'$ lie in a neighborhood of the truth if $\max_{i \in [n]} \|\mathbf{V}'_i - \mathbf{V}_i\|_2$, $\max_{k \in [K]} \|\boldsymbol{\mu}'_k - \boldsymbol{\mu}_k\|_2$, $|\beta'_j - \beta_j|$ for $j = 1, 2, 3$, $\|\mathbf{R}' - \mathbf{R}\|$, and $|\kappa' - \kappa|$ are each bounded above by sufficiently small positive constants.*

Assumption 1 (Number of relational pairs). *(a) The number of observed relatedness pairs n_R satisfies $n_R \gtrsim n \log n$; (b) the number of observed similarity pairs n_S satisfies $n_S \gtrsim \log r$.*

The condition on n_R ensures that, on average, each feature participates in at least a logarithmic number of relatedness pairs, which is sufficient for consistent estimation for $\{\mathbf{V}\}$ from the relatedness signal. The condition on n_S is the minimal threshold for the similarity signal to deliver consistent recovery of $\{\boldsymbol{\mu}\}$. Larger n_R and n_S sharpen the rates for $\{\mathbf{V}\}$ and $\{\boldsymbol{\mu}\}$, respectively (see Theorems 1 and 2 below).

Our analysis requires additional regularity conditions, Assumption 2–4, whose formal statements are deferred to Supplement D. Briefly, Assumption 2 prevents the loading matrices $\{\mathbf{W}\}$, the latent embeddings $\{\mathbf{V}\}$, and the cluster means $\{\boldsymbol{\mu}\}$ from collapsing to lower-dimensional subspaces, and ensures that the relatedness matrix \mathbf{R} is well-conditioned over the neighborhood of the truth. Assumption 3 bounds the similarity and relatedness

logistic probabilities away from 0 and 1, ensuring finite Fisher information. Finally, Assumption 4 ensures local strong convexity of ℓ_{sim} and Lipschitz Hessians for both ℓ_{rel} and ℓ_{sim} , so that the second-order Taylor term dominates the local behavior near the truth. This is a standard condition in non-convex M -estimator analysis (e.g., Balakrishnan et al. 2017; Loh and Wainwright 2015).

3.3 Theoretical Guarantees

The SMILE objective combines three statistically distinct information sources: multi-view linear observations of $\{\mathbf{V}\}$, sparse relational observations defined through logistic models, and a spherical mixture structure that regularizes and anchors the latent geometry. While each component is well studied separately, their joint analysis is nonstandard because the same latent variables enter at different structural levels, and because the relational terms can be highly sparse and heterogeneously sampled. Our theoretical results formalize a key consequence of this construction: the composite estimator adapts to the most informative signal among embeddings, relations, and spherical regularization, while still benefiting when multiple channels are present.

Theorem 1 (Recovery of latent embeddings). *Suppose Assumptions 1–4 hold, and that there exists an orthogonal matrix $\mathbf{O} \in \mathbb{O}^{r \times r}$ such that the SMILE estimator lies in a neighborhood of the truth under the alignment \mathbf{O} . Then there exist choices of the weights w_{rel} and w_{vmf} such that, with probability at least $1 - 10(r)^{-50} - 3(nL)^{-50}$, we have*

$$\frac{1}{n} \sum_{i=1}^n \|\widehat{\mathbf{V}}_i - \mathbf{O}\mathbf{V}_i\|_2^2 \lesssim \frac{\log(nL)}{n} \left(\frac{C_1 \sigma r N^{-1/2} + C_2 w_{\text{rel}} r n_R^{-1/2}}{D_0 N^{-1} + C_3 w_{\text{rel}} n^{-1}} \right)^2 \wedge \left(\frac{r-1}{\kappa} \right),$$

where we define $D_0 \equiv \min_{i \in [n]} |\mathcal{D}_i|$ with $\mathcal{D}_i \equiv \{l \in [L] : i \in \mathcal{S}_l\}$, and C_1, C_2, C_3 are finite positive constants.

The bound in Theorem 1 is non-asymptotic, so $\{\widehat{\mathbf{V}}\}$ is consistent provided that the right-hand side tends to zero. More substantively, the rate captures contributions from all three

information channels: (i) the multi-view embeddings (governed by the level of source overlap quantified by D_0), (ii) relatedness pairs (governed by n_R), and (iii) spherical-mixture regularization (governed by κ); each channel tightens the bound when its underlying signal is strong. The structure of the bound formalizes the heuristic that suitably combining multiple information channels yields a tighter rate than relying on any single one. Corollary 1 below specializes the bound to make the contribution of each channel transparent.

Corollary 1 (Simplified rate for latent embeddings). *Under the same conditions as Theorem 1, with probability at least $1 - 10r^{-50} - 3(nL)^{-50}$, there exists $\mathbf{O} \in \mathbb{O}^{r \times r}$ such that*

$$\frac{1}{n} \sum_{i=1}^n \|\widehat{\mathbf{V}}_i - \mathbf{O}\mathbf{V}_i\|_2^2 \lesssim \left(\frac{r^2 N \log(nL)}{D_0^2 n} \right) \wedge \left(\frac{r^2 n \log(nL)}{n_R} \right) \wedge \left(\frac{r-1}{\kappa} \right).$$

The first term is the multi-view baseline obtained by setting $w_{\text{rel}} = w_{\text{vmf}} = 0$. It captures the error incurred when estimating $\{\mathbf{V}\}$ solely from the observed embeddings $\{\mathbf{U}\}$ across heterogeneous sources. The dependence on D_0 shows that a higher level of source overlap acts as a larger effective sample size, tightening the bound.

The second term is attained as $w_{\text{rel}} \rightarrow \infty$, i.e., from relatedness pairs alone. It is smaller than the first term when $n_R \gtrsim D_0^2 n^2 / N$, i.e., when the observed relatedness graph is dense enough that the relatedness-only rate beats the multi-view baseline. In practice this threshold is mild: in the fully-overlapping regime ($N = Ln, D_0 = L$) it simplifies to $n_R \gtrsim Ln$, which is attainable whenever the relatedness graph has any non-vanishing density. Therefore, even sparse relational supervision delivers rate-level improvement over the multi-view baseline.

The final term, reached as $w_{\text{vmf}} \rightarrow \infty$, reflects the regularization effect induced by the vMF prior on the latent embeddings. This term becomes active when the concentration parameter κ is large, corresponding to highly informative spherical structure.

In summary, SMILE benefits from multi-channel integration: jointly leveraging heterogeneous information tightens the rate on $\{\mathbf{V}\}$ beyond what any single channel could

achieve alone.

We next control the estimation of the cluster mean directions $\{\boldsymbol{\mu}\}$.

Theorem 2 (Recovery of cluster mean directions). *Suppose Assumptions 1–4 hold, and that there exists an orthogonal matrix $\mathbf{O} \in \mathbb{O}^{r \times r}$ such that the SMILE estimator lies in a neighborhood of the truth under the alignment \mathbf{O} . With probability at least $1 - 3r^{-10}$, we have*

$$\frac{1}{K} \sum_{k=1}^K \|\widehat{\boldsymbol{\mu}}_k - \mathbf{O}\boldsymbol{\mu}_k\|_2^2 \lesssim \left(\frac{r^2 \log r}{n_S} \right) \wedge \left(\frac{Kr}{n\kappa} \right).$$

The rate in Theorem 2 reflects two complementary information sources for recovering the cluster mean directions $\{\boldsymbol{\mu}\}$: similarity pairs (quantified by n_S) and the concentration of the spherical mixture (governed by κ). The bound tightens as either channel becomes more informative, which can be achieved through more observed similarity pairs or higher concentration κ .

Finally, we turn to clustering. Our analysis follows a standard margin-based argument commonly used in classification and mixture model theory (see e.g., Tsybakov 2004; Fromont and Tuleau 2006). Define the (population) margin for feature i by

$$m_i \equiv \log \pi_{iz_i} + \kappa \boldsymbol{\mu}_{z_i}^\top \mathbf{V}_i - \max_{k \neq z_i} (\log \pi_{ik} + \kappa \boldsymbol{\mu}_k^\top \mathbf{V}_i),$$

which quantifies separation between the true component and its closest competitor. Since misclassification is concentrated on features near the decision boundary, the next theorem shows that consistent clustering follows once the estimation errors are small relative to the typical margin.

Theorem 3 (Clustering consistency). *Let E_V^2 and E_μ^2 be upper bounds for $\frac{1}{n} \sum_{i=1}^n \|\widehat{\mathbf{V}}_i - \mathbf{O}\mathbf{V}_i\|_2^2$ and $\frac{1}{K} \sum_{k=1}^K \|\widehat{\boldsymbol{\mu}}_k - \mathbf{O}\boldsymbol{\mu}_k\|_2^2$, respectively, as provided by Theorems 1 and 2. Suppose there exist finite positive constants c_V, c_μ such that $E_V^2/c_V^2 = o(1)$ and $E_\mu^2/c_\mu^2 = o(1)$. If*

$$\frac{1}{n} \left| \{i \in [n] : m_i \leq 2\kappa(c_V + c_\mu)\} \right| \rightarrow 0,$$

then there exists a permutation τ of $[K]$ such that

$$\frac{1}{n} \sum_{i=1}^n \mathbb{1}\{\tau(\hat{z}_i) = z_i\} \rightarrow 1.$$

Theorem 3 establishes clustering consistency under two conditions: (i) the latent embeddings and cluster mean directions are estimated accurately enough, and (ii) the proportion of features with small margins (i.e., those near the decision boundary) vanishes. The first condition is delivered by Theorems 1 and 2. The second is a structural condition on the population requiring most features to be unambiguously assignable to their clusters. Together, these ensure that the misclassification rate (up to permutation) converges to zero, formalizing how SMILE consistently recovers the latent synonym groups.

Overall, Theorems 1, 2, and 3 characterize how SMILE’s three estimation tasks (latent embeddings, cluster mean directions, and cluster memberships) depend on the strength of each information channel. Stronger multi-view supervision, more relational pairs, and/or stronger spherical concentration tighten the embedding and mean direction rates, which in turn relax the margin requirement for consistent clustering.

4 Simulation Studies

We have conducted extensive simulation studies to evaluate the finite-sample performance of SMILE. We specifically examine how estimation and clustering performance depend on the number of embedding sources L , the spherical concentration parameter κ , the number of clusters K , and the amount of relational supervision. We compare SMILE against three multi-view integration baselines: SVD applied to concatenated embeddings, AJIVE (Angle-based Joint and Individual Variation Explained; Feng et al. 2018), and SLIDE (Structural Learning and Integrative DEcomposition of multi-view data; Gaynanova and Li 2019). Since these methods only estimate embeddings and cannot directly infer cluster membership, we pair each with k -means and hierarchical clustering to yield six

competing procedures. Cluster centers are then computed using normalized within-cluster averages, followed by permutation alignment. All reported results are based on 100 Monte Carlo replications for each configuration.

Throughout, we consider $n = 1000$ unique features and assign them to $K \in \{50, 100\}$ clusters via a uniform multinomial distribution, resulting in probabilistically balanced cluster sizes. The elements of the cluster centers $\{\boldsymbol{\mu}\}$ in the $r = 6$ dimensional latent space are drawn independently from $\mathcal{N}(1/\sqrt{6}, 1)$ and then each vector $\boldsymbol{\mu}_k$ is normalized to have unit norm. Conditional on $\{\boldsymbol{\mu}\}$ and $\{z\}$, the latent embeddings $\{\mathbf{V}\}$ are generated from vMF distributions with concentration parameter $\kappa \in \{100, 150, 200\}$. We consider $L \in \{2, 3, 4\}$ sources, with feature sets $\mathcal{S}_1 = \{1, \dots, 1000\}$, $\mathcal{S}_2 = \{1, \dots, 500\}$, $\mathcal{S}_3 = \{301, \dots, 800\}$, and $\mathcal{S}_4 = \{501, \dots, 1000\}$. Moreover, all source-specific embeddings $\{\mathbf{U}\}$ have dimension $r_l = 200$, and are generated from vMF distributions with mean direction $\mathbf{W}_l \mathbf{V}_i / \|\mathbf{W}_l \mathbf{V}_i\|_2$ and concentration parameter 60, where \mathbf{W}_l has entries drawn independently from $\mathcal{N}(0.6, 1)$.

Because our sources only partially overlap but the competing methods require complete embedding matrices, we impute the missing embeddings. Since \mathcal{S}_1 contains all features, we perform SVD on $\{\mathbf{U}_i^{(1)}\}$ and then map the resulting embeddings into the space of source $l \in \{2, 3, 4\}$ using an orthogonal Procrustes transformation estimated from the observed $\{\mathbf{U}_i^{(l)}\}$. In contrast, SMILE naturally accommodates partially overlapping feature spaces and does not require imputation.

For SMILE, we additionally generated similarity and relatedness edges according to the logistic models (3) and (4) with $\beta_1 = -0.125$, $\beta_2 = 5$, $\beta_3 = -0.125$, and $\mathbf{R} = \text{diag}(5, \dots, 5)$. Among all positive pairs, we retain only a random subset as observed. For negative pairs, we select “hard negatives” with the largest cosine similarities (based on first-source embeddings). We vary the overall proportion of observed relational pairs as follows: (i) 4% similarity and 4% relatedness (both with 1.5% positive, 2.5% negative); (ii) 6% similarity and 6% relatedness (both with 2.5% positive, 3.5% negative); and (iii) 8% similarity and

8% relatedness (both with 3.5% positive, 4.5% negative).

SMILE also incorporates prior correspondence information through $\{\pi_{ik}\}$. To emulate such information, we treat 70% of the clusters as anchor clusters, containing approximately 70% of all features with known memberships. We transform these anchor relations into soft cluster-assignment probabilities using a spectral-clustering-based procedure (see Supplement A for details). Clustering accuracy for all methods is evaluated on the remaining 30% of features in the 30% non-anchor clusters.

We considered the following settings for comparison:

- **Setting 1: Varying the number of embedding sources L .** We evaluate each method for $L \in \{2, 3, 4\}$, using feature sets $\{\mathcal{S}_l : l \in [L]\}$, while fixing $\kappa = 150$, $K = 50$, and 6% observed relational pairs for SMILE.
- **Setting 2: Varying the concentration parameter κ in the vMF distributions.** We consider $\kappa \in \{100, 150, 200\}$, while fixing $L = 3$ with feature sets $\{\mathcal{S}_l : l \in [L]\}$, $K = 50$, and 6% observed relational pairs for SMILE.
- **Setting 3: Varying the number of clusters K .** We consider $K \in \{50, 100\}$, while fixing $L = 3$ with feature sets $\{\mathcal{S}_l : l \in [L]\}$, $\kappa = 150$, and 6% observed relational pairs for SMILE.
- **Setting 4: Varying the amount of relational supervision used by SMILE.** We consider $\{4\%, 6\%, 8\%\}$ observed relational pairs for SMILE, while fixing $L = 3$ with feature sets $\{\mathcal{S}_l : l \in [L]\}$, $\kappa = 150$, and $K = 50$.

To assess how well each method recovers the true latent embeddings (up to rotation), we define an accuracy metric

$$\text{RelAcc}(\mathbf{V}) = \frac{1}{1 + \text{RelErr}(\mathbf{V})} \quad \text{with} \quad \text{RelErr}(\mathbf{V}) = \frac{\|\widehat{\mathbf{V}}\widehat{\mathbf{V}}^\top - \mathbf{V}_0\mathbf{V}_0^\top\|_F}{\|\mathbf{V}_0\mathbf{V}_0^\top\|_F},$$

where $\widehat{\mathbf{V}}$ and \mathbf{V}_0 are the $n \times r$ estimated and true embedding matrices. Cluster-mean accuracy is defined analogously, using permutation-aligned estimated clusters. Clustering accuracy is evaluated by adjusted mutual information (AMI), which adjusts for chance agreement and ranges from 0 to 1.

Figure 1 summarizes the estimation and clustering performance of all methods in Settings 1–3. The main conclusion is that SMILE consistently achieves the best performance across all settings and tasks, highlighting the benefit of jointly leveraging relational supervision and prior information to refine embeddings and recover cluster means and memberships. More specifically, for the estimation of the latent embeddings $\{\mathbf{V}\}$, AJIVE and SVD perform comparably, while SLIDE underperforms, likely due to its structural assumptions; SMILE attains the highest accuracy in every setting. For the accuracy of cluster means $\{\boldsymbol{\mu}\}$ and membership recovery, k -means generally outperforms hierarchical clustering when paired with the same embeddings, yet SMILE still clearly outperforms all competitors. As the number of embedding sources L increases, all methods improve because additional views provide more information about the latent structure. As the vMF concentration κ increases, performance again improves for all methods, most prominently for SMILE, since higher concentration yields more tightly clustered embeddings. In contrast, increasing the number of clusters K makes the estimation and clustering more challenging, so all methods deteriorate, but SMILE remains the top performer. Notably, when $K = 100$, there are on average 10 codes per cluster, a scenario close to what we see in practice (e.g., the real data application in Section 5), and SMILE maintains a clear advantage, demonstrating its robustness in realistic high-resolution clustering settings.

Figure S1 in Supplement B reports the results for Setting 4. Because competing methods do not use relational pairs, their performance remains unchanged, whereas SMILE outperforms them even with the sparsest relational labels and exhibits improving estimation and clustering accuracy as more relational information becomes available, in line with

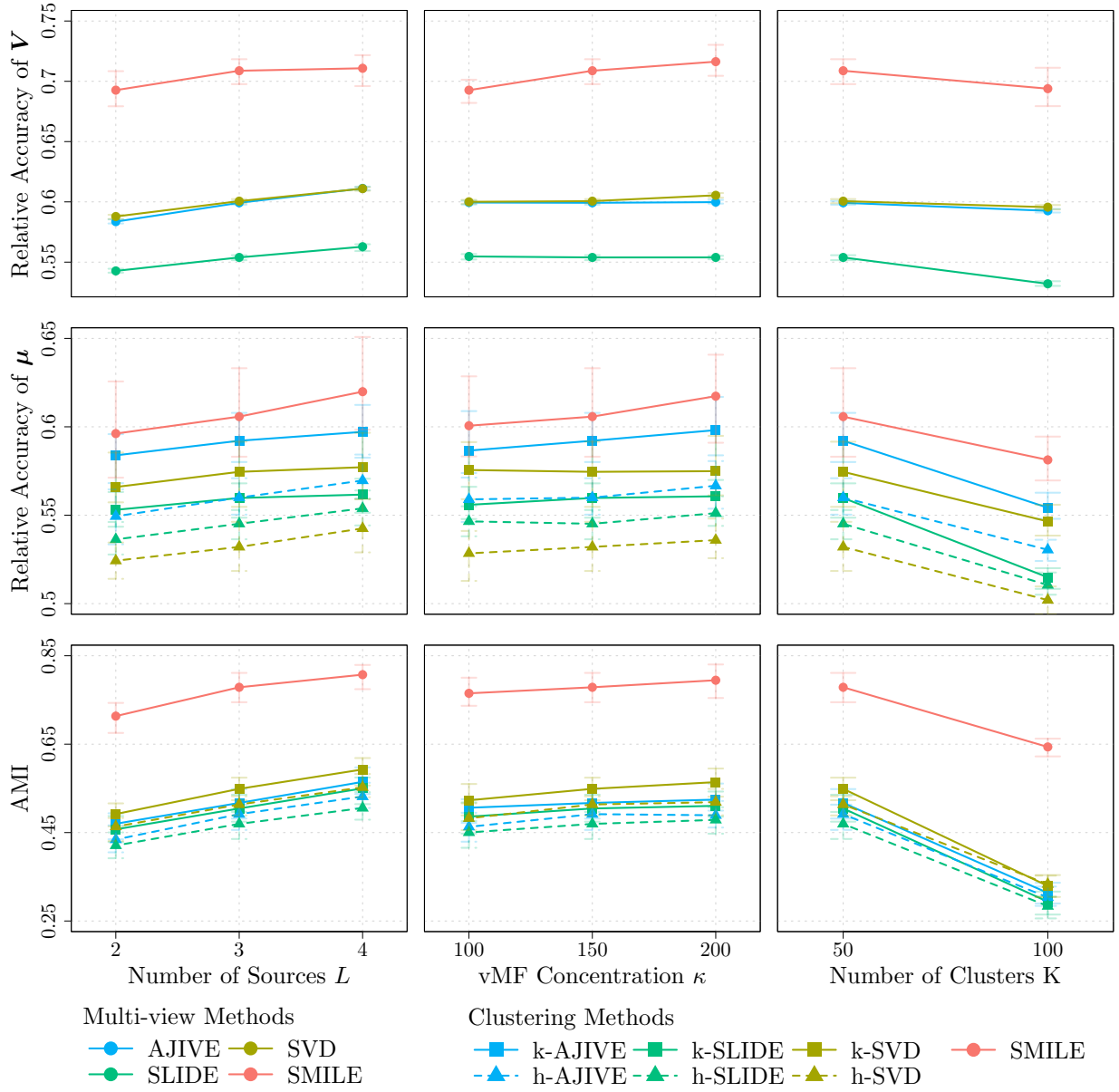


Figure 1: Empirical performance of multi-view integration and clustering methods across three simulation settings. Columns correspond to (left) Setting 1: varying the number of embedding sources L ; (middle) Setting 2: varying the vMF concentration κ ; and (right) Setting 3: varying the number of clusters K . Rows report relative accuracy of the latent embeddings \mathbf{V} (top), relative accuracy of cluster centers $\boldsymbol{\mu}$ (middle), and clustering accuracy measured by AMI (bottom). “k-XXX” and “h-XXX” refer to method XXX (SVD, AJIVE, or SLIDE) combined with k -means and hierarchical clustering, respectively.

the theoretical rates.

5 Real Data Analysis

We evaluate SMILE using real-world EHR data from Mass General Brigham (MGB) and Veteran Affairs (VA), with the goal of harmonizing and grouping clinical codes through the integration of EHR-derived embeddings and language-based embeddings of those codes. Our evaluation focuses on two complementary objectives. First, we assess whether SMILE yields higher-quality latent embeddings than existing multi-view integration methods, using downstream tasks that measure recovery of known similarity/relatedness relationships and identification of disease-relevant features. Second, we examine whether SMILE improves clustering of synonymous or hierarchically related codes, particularly for aligning institution-specific codes to standardized ontologies. As in the simulations, we compare SMILE to SVD, AJIVE, and SLIDE for learning latent embeddings, and to each of these methods combined with k -means or hierarchical clustering for feature clustering.

We begin by describing the MGB and VA EHR datasets used in our analysis. The raw EHR codes were first standardized by mapping highly granular codes to higher level code concepts, following the approach described in Hong et al. (2021). From MGB, we include diagnosis mapped to PheCodes, medications mapped to RxNorm codes, and laboratory tests mapped to LOINC codes. From VA, we include the same three ontologies, along with two additional VA-specific laboratory codes, granular local lab codes (“OtherLab”) and grouped lab codes (“ShortName”). To increase cluster sizes and strengthen relational structure for embedding estimation, we further augment the dataset with additional PheCodes and RxNorm codes that share parents with existing MGB and VA codes. A summary of the resulting feature counts is provided in Table 1.

We incorporate $L = 4$ embedding sources. Two are co-occurrence-based PMI-SVD

	PheCode	RxNorm	LOINC	OtherLab	ShortName	Total
MGB only	63	252	616	0	0	931
VA only	45	504	215	1814	94	2672
Overlap	1730	810	167	0	0	2707
Additionally added	26	1112	0	0	0	1138
Total	1864	2678	998	1814	94	7448

Table 1: Summary of feature counts on the MGB and VA EHR datasets.

embeddings (1500 dimensions each), computed separately from the MGB and VA EHR systems and therefore available only for codes observed at the corresponding institution. The remaining two are description-based embeddings derived from PLMs: SapBERT (768 dimensions; Liu et al. 2020) and BGE (1024 dimensions; Chen et al. 2024), which are available for all codes. By combining EHR co-occurrence structure with semantic representations learned from biomedical text, we aim to jointly capture institution-specific usage patterns and cross-institution semantic consistency.

Since PMI-SVD embeddings are missing for codes not observed at a given institution, competing methods that require complete embedding matrices are applied to imputed PMI-SVD representations. Specifically, we first apply SVD to concatenated SapBERT–BGE embeddings and then map the resulting representations into the PMI space via an orthogonal Procrustes transformation estimated using codes with observed PMI-SVD embeddings. In contrast, SMILE is trained directly on the original (non-imputed) embeddings, allowing it to accommodate heterogeneous, partially overlapping feature spaces without imputation.

To limit information leakage, we partition codes into training, validation, and test sets. For ontology-based codes (PheCode, RxNorm, and LOINC), the split is performed at the level of ontology parents so that all codes sharing a parent remain in the same subset. VA local laboratory codes (OtherLab and ShortName), which lack comparable hierarchies, are

randomly assigned. The resulting split ratio is approximately 70/10/20, with feature counts summarized in Table 2. All codes enter SMILE through their source-specific embeddings.

	PheCode	RxNorm	LOINC	OtherLab	ShortName	Total
Training	1348	1795	703	1303	70	5219
Validation	100	330	91	219	8	748
Test	416	553	204	292	16	1481
Total	1864	2678	998	1814	94	7448

Table 2: Summary of feature counts in the training, validation and test sets.

For evaluation, we leverage the hierarchical structure of PheCode, RxNorm, and LOINC to define cluster targets. Two PheCodes are clustered together if they share the same integer parent; RxNorm codes are grouped by one-level-up Anatomical Therapeutic Chemical (ATC) class (Nahler, 2009); and LOINC codes are grouped using first-level LOINC PART (LP) codes. VA-specific laboratory codes are mapped to these LP parents via curated OMOP relationships. The resulting clustering is highly granular: cluster sizes range from 1 to 25, with 41% of codes in clusters of size at most 5 and 68% in clusters of size at most 10. The number of clusters per category is selected by maximizing the Silhouette coefficient on k -means applied to SVD embeddings, yielding 600 clusters for PheCode, 570 for RxNorm, and 730 for laboratory codes, for a total of $K = 1900$. SMILE accepts a structured $n \times K$ prior probability matrix $\{\pi_{ik}\}$ that encodes partial cluster knowledge, in contrast to benchmark methods that cluster features separately within each category. For training codes, we treat their cluster memberships as known and set a hard prior with $\pi_{ik} = 1$ on the true cluster and 0 elsewhere. For validation and test codes, their true memberships are withheld from SMILE: validation memberships are reserved for hyperparameter tuning, and test memberships for final evaluation. For these codes, their priors are constructed by combining GPT-4-proposed candidate same-cluster pairs (Supplement C) with spectral

clustering under soft probabilistic assignments (Supplement A). The resulting per-category probability matrices then stack into the block-structured prior matrix $\{\pi_{ik}\}$.

Similar pairs are constructed using ontology structure and mappings from the Unified Medical Language System (UMLS). With ontology hierarchies, two codes are labeled similar if they are first cousins, or if one code’s parent is the other’s grandparent. “Hard negative” pairs are defined if two codes are second cousins, or if one code’s great-grandparent is the other’s parent or grandparent. We further augment the positive set with established biomedical relationships from UMLS. To enrich the negative set, we sample pairs that are not ontology/UMLS positives but exhibit relatively high cosine similarity based on CODER embeddings. In total, approximately 6% of code pairs are labeled as positive or negative similar pairs. Relatedness pairs are constructed similarly, incorporating UMLS and GPT-4-generated silver-standard labels (detailed procedure and prompt in Supplement C); approximately 6% of code pairs are labeled. All labeled pairs are then split into train, validation, and test sets. Training pairs are those with both codes in the training set; they comprise 58% of all pairs and provide the only supervision SMILE receives. The remaining 42% (with at least one held-out code) are randomly partitioned 25/75 into a validation set (10% of all pairs, reserved for hyperparameter tuning) and a test set (32%, reserved for final evaluation).

Since latent embedding quality and feature clustering quality reflect different levels of the model (feature- versus cluster-level) and admit no common optimum, we tune hyperparameters to balance both criteria rather than optimize either alone. Specifically, we evaluate each candidate configuration on the validation set using (i) the average clustering AMIs across PheCode, RxNorm, and laboratory categories on validation features, and (ii) the average areas under the ROC curves (AUCs) across similarity and relatedness on validation pairs. We select a configuration on the Pareto frontier of these two criteria, with selected latent dimension $r = 60$. All methods are evaluated on the same test pairs and test

features; since these test sets are not used during any method’s training or hyperparameter selection, the comparison across methods is fair.

5.1 Evaluating the Quality of Latent Embeddings

We evaluate embedding quality through two downstream tasks: recovery of known similarity/relatedness relationships and selection of disease-relevant features.

For the first task, we treat known similar/related pairs as positives and random pairs as negatives, and compute the AUC using embedding-based pairwise scores. For all benchmark methods, the score for a pair (i, j) is the cosine similarity of the estimated feature-level embeddings $\widehat{\mathbf{V}}_i$ and $\widehat{\mathbf{V}}_j$, used for both similarity and relatedness AUC. For SMILE, the similarity score is likewise the cosine similarity of $\widehat{\mathbf{V}}_i$ and $\widehat{\mathbf{V}}_j$; the relatedness score is the cosine similarity of $\widehat{\mathbf{R}}^{1/2}\widehat{\mathbf{V}}_i$ and $\widehat{\mathbf{R}}^{1/2}\widehat{\mathbf{V}}_j$, reflecting the bilinear form in (4).

Results in Table 3 show that all multi-view methods achieve relatively strong similarity AUCs. The imputed institutional embeddings (MGB-PMI and VA-PMI) already perform competitively, which is unsurprising given that the imputation step itself fuses institutional co-occurrence information with PLM semantics via Procrustes alignment, thereby effectively combining two complementary information sources. SMILE matches or marginally exceeds the strongest baseline, and importantly does so without requiring an imputation step: it operates directly on the original partially overlapping vocabularies. This pattern reflects that ontology-defined similarity pairs are largely recoverable from well-integrated low-rank structure. However, the harder discriminative signal lies in the relatedness pairs. SMILE lifts relatedness AUC from 0.7762 to 0.9455 on the test set, a 22% relative gain over SLIDE, the strongest baseline. Relatedness pairs span ontology branches and probe broader functional associations (e.g., between a disease and its treatment) that low-rank decomposition does not model directly, whereas SMILE’s bilinear relatedness model captures these cross-cluster geometric relationships explicitly.

		MGB-PMI	VA-PMI	SapBERT	BGE	SVD	AJIVE	SLIDE	SMILE
Sim	Train	0.8927	0.9106	0.7787	0.7841	0.8928	0.9140	0.9134	0.9167
	Test	0.8562	0.8780	0.7340	0.7474	0.8583	0.8838	0.8828	0.8878
Rel	Train	0.7628	0.7894	0.7506	0.6849	0.7664	0.7957	0.8016	0.9459
	Test	0.7236	0.7670	0.7053	0.6606	0.7281	0.7686	0.7762	0.9455

Table 3: AUC comparison across embedding sources and methods. Train pairs are used for SMILE supervision, and test pairs are the 75% of held-out pairs reserved for evaluation; the remaining 25% of held-out pairs form the validation set used only for hyperparameter tuning and are not reported here. “MGB-PMI” and “VA-PMI” refer to imputed PMI-SVD embeddings derived from the MGB and VA EHR systems, respectively. “Sim” and “Rel” refer to similarity-based and relatedness-based labels, respectively.

For the second task, we randomly select 11 PheCodes that appear in both the MGB and VA data as target diseases. For each disease, we construct a candidate feature set by taking the top 100 features across categories according to the aforementioned embeddings and augmenting them with 100 randomly sampled features as negative controls. For each embedding method, we compute the embedding cosine similarity between each candidate feature and the target disease as the feature’s relevance score, and in parallel obtain GPT-4 semantic relevance scores based on textual feature descriptions. We then quantify agreement between embedding-based and GPT-4-based rankings using Spearman’s rank correlation. Averaged over the 11 target diseases, the correlations are SVD = 0.4283, AJIVE = 0.4110, SLIDE = 0.4064, and SMILE = 0.4407, indicating that SMILE provides the most informative embeddings for identifying disease-relevant features.

5.2 Clustering and Code Harmonization

Clustering performance on the test set is measured by AMI, which is robust to many small, imbalanced clusters. Results for all methods are summarized in Table 4.

	<i>k</i> -means			hclust			
	SVD	AJIVE	SLIDE	SVD	AJIVE	SLIDE	SMILE
PheCode	0.2337	0.2395	0.2379	0.2364	0.2372	0.2304	0.3994
RxNorm	0.0801	0.0936	0.0860	0.0641	0.0765	0.0833	0.1703
Lab	0.0685	0.0716	0.0718	0.0427	0.0623	0.0613	0.1597
LOINC	0.0590	0.0669	0.0676	0.0394	0.0617	0.0606	0.1135
VA local lab	0.0559	0.0574	0.0582	0.0312	0.0521	0.0511	0.1659

Table 4: AMI of clustering performance on the test features for different methods. “hclust” refers to hierarchical clustering. “Lab” includes both LOINC codes and VA local laboratory codes (OtherLab and ShortName). “VA local lab” only includes VA local laboratory codes.

The ontology-based clustering problem is intrinsically difficult, with highly imbalanced cluster sizes and most codes in very small groups; in this setting, even a few misassignments create many pairwise disagreements and strongly depress chance-adjusted indices such as AMI, so even good methods rarely approach an AMI of 1. Across baselines, *k*-means and hierarchical clustering on SVD, AJIVE, and SLIDE yield broadly similar AMIs, indicating that existing multi-view methods offer limited benefit for recovering these fine-grained ontology clusters. In contrast, SMILE consistently outperforms all baselines: it improves AMI from 0.2395 to 0.3994 for PheCode (about 67% gain), 0.0936 to 0.1703 for RxNorm (about 82% gain), 0.0718 to 0.1597 for all lab codes (about 122% gain), and 0.0676 to 0.1135 for LOINC (about 68% gain). PheCode attains higher AMI because diagnosis clusters are coarser and more coherent than the more heterogeneous, fine-grained medication and

lab clusters. Notably, for VA local laboratory codes, SMILE raises AMI from 0.0582 to 0.1659 (about 185% gain), underscoring its utility for mapping institution-specific codes to standardized ontologies.

6 Conclusion

Multi-institutional studies face persistent interoperability challenges due to partially overlapping coding systems and heterogeneous data modalities. SMILE addresses this by learning a unified embedding space that integrates co-occurrence pattern, semantic embeddings, and biomedical knowledge. Rather than treating harmonization as a post-hoc mapping problem, SMILE aligns institution-specific codes directly within a shared latent representation, automatically harmonizing synonymous or related features across sites. This unified space enables patients to be represented using harmonized feature embeddings, mitigating coding discrepancies at the representation level and allowing downstream analyses to operate on semantically aligned patient profiles rather than institution-specific codes.

Importantly, this framework is extensible beyond structured codes. Because SMILE operates at the embedding level, it can naturally incorporate narrative concepts extracted from clinical notes, such as symptom phrases, problem list entries, or contextual modifiers derived from large language models. Integrating structured codes and narrative-derived concepts within a unified embedding space would further reduce modality-specific fragmentation and move toward fully automated, representation-driven EHR harmonization. In this sense, SMILE provides not only improved clustering and embedding performance, but also a scalable infrastructure for cross-institutional, multi-modal patient representation in clinical and translational research.

References

- Alaux, J., E. Grave, M. Cuturi, and A. Joulin (2018). Unsupervised hyperalignment for multilingual word embeddings. *arXiv preprint arXiv:1811.01124*.
- Arora, S., Y. Li, Y. Liang, T. Ma, and A. Risteski (2015). A latent variable model approach to pmi-based word embeddings. *arXiv preprint arXiv:1502.03520*.
- Balakrishnan, S., M. J. Wainwright, and B. Yu (2017). Statistical guarantees for the EM algorithm: From population to sample-based analysis. *The Annals of Statistics* 45(1), 77–120.
- Bao, R., Y. Sun, Y. Gao, J. Wang, Q. Yang, Z.-H. Mao, and Y. Ye (2023). A recent survey of heterogeneous transfer learning. *arXiv preprint arXiv:2310.08459*.
- Barbaro, F. and F. Rossi (2021). Sparse mixture of von mises-fisher distribution. In *2021 European Symposium on Artificial Neural Networks, Computational Intelligence and Machine Learning*.
- Bianchi, D. W., P. F. Brennan, M. F. Chiang, L. A. Criswell, R. N. D’Souza, G. H. Gibbons, J. K. Gilman, J. A. Gordon, E. D. Green, S. Gregurick, et al. (2024). The all of us research program is an opportunity to enhance the diversity of us biomedical research. *Nature Medicine* 30(2), 330–333.
- Brämer, G. R. (1988). International statistical classification of diseases and related health problems. Tenth revision. *World Health Statistics Quarterly. Rapport Trimestriel de Statistiques Sanitaires Mondiales* 41(1), 32–36.
- Brat, G. A., G. M. Weber, N. Gehlenborg, P. Avillach, N. P. Palmer, L. Chiovato, J. Cimino, L. R. Waitman, G. S. Omenn, A. Malovini, et al. (2020). International electronic health record-derived covid-19 clinical course profiles: the 4ce consortium. *NPJ Digital Medicine* 3(1), 109.
- Chen, J., S. Xiao, P. Zhang, K. Luo, D. Lian, and Z. Liu (2024). Bge m3-embedding: Multilingual, multi-functionality, multi-granularity text embeddings through self-knowledge distillation. *arXiv preprint arXiv:2402.03216* 4(5).

- Choi, D. S., P. J. Wolfe, and E. M. Airoidi (2012). Stochastic blockmodels with a growing number of classes. *Biometrika* 99(2), 273–284.
- Choi, E., M. T. Bahadori, E. Searles, C. Coffey, M. Thompson, J. Bost, J. Tejedor-Sojo, and J. Sun (2016). Multi-layer representation learning for medical concepts. In *Proceedings of the 22nd ACM SIGKDD International Conference on Knowledge Discovery and Data Mining*, pp. 1495–1504.
- Day, O. and T. M. Khoshgoftaar (2017). A survey on heterogeneous transfer learning. *Journal of Big Data* 4(1), 29.
- Feng, Q., M. Jiang, J. Hannig, and J. Marron (2018). Angle-based joint and individual variation explained. *Journal of Multivariate Analysis* 166, 241–265.
- Feuz, K. D. and D. J. Cook (2015). Transfer learning across feature-rich heterogeneous feature spaces via feature-space remapping (fsr). *ACM Transactions on Intelligent Systems and Technology*.
- Fromont, M. and C. Tuleau (2006). Functional classification with margin conditions. In *International Conference on Computational Learning Theory*, pp. 94–108. Springer.
- Gan, Z., D. Zhou, E. Rush, V. A. Panickan, Y.-L. Ho, G. Ostrouchovm, Z. Xu, S. Shen, X. Xiong, K. F. Greco, et al. (2025). Arch: Large-scale knowledge graph via aggregated narrative codified health records analysis. *Journal of Biomedical Informatics* 162, 104761.
- Garcia, B., M. Hogarth, Y. Wang, X. Zhu, and S.-P. Tu (2025). Multi-site research using electronic health record data: Lessons learned from a case study. *Learning Health Systems* 9(4), e70039.
- Gaynanova, I. and G. Li (2019). Structural learning and integrative decomposition of multi-view data. *Biometrics* 75(4), 1121–1132.
- Gopal, S. and Y. Yang (2014). Von mises-fisher clustering models. In *International Conference on Machine Learning*, pp. 154–162. PMLR.

- Grave, E., A. Joulin, and Q. Berthet (2019). Unsupervised alignment of embeddings with wasserstein procrustes. In *The 22nd International Conference on Artificial Intelligence and Statistics*, pp. 1880–1890. PMLR.
- Holland, P. W., K. B. Laskey, and S. Leinhardt (1983). Stochastic blockmodels: First steps. *Social Networks* 5(2), 109–137.
- Hong, C., E. Rush, M. Liu, D. Zhou, J. Sun, A. Sonabend, V. M. Castro, P. Schubert, V. A. Panickan, T. Cai, et al. (2021). Clinical knowledge extraction via sparse embedding regression (keser) with multi-center large scale electronic health record data. *NPJ Digital Medicine* 4(1), 151.
- Hu, Y. and W. Wang (2024). Network-adjusted covariates for community detection. *Biometrika* 111(4), 1221–1240.
- Lei, J. and A. Rinaldo (2015). Consistency of spectral clustering in stochastic block models. *The Annals of Statistics*, 215–237.
- Li, M., X. Li, K. Pan, A. Geva, D. Yang, S. M. Sweet, C.-L. Bonzel, V. Ayakulangara Panickan, X. Xiong, K. Mandl, et al. (2024). Multisource representation learning for pediatric knowledge extraction from electronic health records. *NPJ Digital Medicine* 7(1), 319.
- Li, S., P. Liu, G. G. Nascimento, X. Wang, F. R. M. Leite, B. Chakraborty, C. Hong, Y. Ning, F. Xie, Z. L. Teo, et al. (2023). Federated and distributed learning applications for electronic health records and structured medical data: a scoping review. *Journal of the American Medical Informatics Association* 30(12), 2041–2049.
- Liu, F., E. Shareghi, Z. Meng, M. Basaldella, and N. Collier (2020). Self-alignment pretraining for biomedical entity representations. *arXiv preprint arXiv:2010.11784*.
- Liu, S., W. Ma, R. Moore, V. Ganesan, and S. Nelson (2005). Rxnorm: prescription for electronic drug information exchange. *IT Professional* 7(5), 17–23.

- Lock, E. F., K. A. Hoadley, J. S. Marron, and A. B. Nobel (2013). Joint and individual variation explained (jive) for integrated analysis of multiple data types. *The Annals of Applied Statistics* 7(1), 523.
- Lock, E. F., J. Y. Park, and K. A. Hoadley (2022). Bidimensional linked matrix factorization for pan-omics pan-cancer analysis. *The Annals of Applied Statistics* 16(1), 193.
- Loh, P.-L. and M. J. Wainwright (2015). Regularized M-estimators with nonconvexity: Statistical and algorithmic theory for local optima. *Journal of Machine Learning Research* 16, 559–616.
- Ma, C., K. Wang, Y. Chi, and Y. Chen (2020). Implicit regularization in nonconvex statistical estimation: Gradient descent converges linearly for phase retrieval, matrix completion, and blind deconvolution. *Foundations of Computational Mathematics* 20(3), 451–632.
- Marwaha, J. S., M. Downing, J. Halamka, A. Abernethy, J. B. Franklin, B. Anderson, I. Kohane, K. Wagholikar, J. Brownstein, M. Haendel, et al. (2024). Mobilizing data during a crisis: Building rapid evidence pipelines using multi-institutional real world data. In *Healthcare*, Volume 12, pp. 100738. Elsevier.
- McDonald, C. J., S. M. Huff, J. G. Suico, G. Hill, D. Leavelle, R. Aller, A. Forrey, K. Mercer, G. DeMoor, J. Hook, et al. (2003). Loinc, a universal standard for identifying laboratory observations: a 5-year update. *Clinical Chemistry* 49(4), 624–633.
- Nahler, G. (2009). Anatomical therapeutic chemical classification system (atc). In *Dictionary of Pharmaceutical Medicine*, pp. 8–8. Springer.
- Park, J. Y. and E. F. Lock (2020). Integrative factorization of bidimensionally linked matrices. *Biometrics* 76(1), 61–74.
- Pei, S., L. Yu, G. Yu, and X. Zhang (2022). Graph alignment with noisy supervision. In *Proceedings of the ACM Web Conference*, pp. 1104–1114.

- Rohe, K., S. Chatterjee, and B. Yu (2011). Spectral clustering and the high-dimensional stochastic blockmodel. *The Annals of Statistics* 39(4), 1878–1915.
- Shi, X., X. Li, and T. Cai (2021). Spherical regression under mismatch corruption with application to automated knowledge translation. *Journal of the American Statistical Association* 116(536), 1953–1964.
- Si, Y., J. Du, Z. Li, X. Jiang, T. Miller, F. Wang, W. J. Zheng, and K. Roberts (2021). Deep representation learning of patient data from electronic health records (ehr): A systematic review. *Journal of Biomedical Informatics* 115, 103671.
- Sittig, D. F., B. L. Hazlehurst, J. Brown, S. Murphy, M. Rosenman, P. Tarczy-Hornoch, and A. B. Wilcox (2012). A survey of informatics platforms that enable distributed comparative effectiveness research using multi-institutional heterogeneous clinical data. *Medical Care* 50, S49–S59.
- Tsybakov, A. B. (2004). Optimal aggregation of classifiers in statistical learning. *The Annals of Statistics* 32(1), 135–166.
- Wang, Z., Q. Gu, Y. Ning, and H. Liu (2015). High dimensional EM algorithm: Statistical optimization and asymptotic normality. In *Advances in Neural Information Processing Systems*, pp. 2521–2529.
- Yang, Z. and G. Michailidis (2016). A non-negative matrix factorization method for detecting modules in heterogeneous omics multi-modal data. *Bioinformatics* 32(1), 1–8.
- Yi, S., R. K. W. Wong, and I. Gaynanova (2023). Hierarchical nuclear norm penalization for multi-view data integration. *Biometrics* 79(4), 2933–2946.
- Yuan, Z., Z. Zhao, H. Sun, J. Li, F. Wang, and S. Yu (2022). Coder: Knowledge-infused cross-lingual medical term embedding for term normalization. *Journal of Biomedical Informatics* 126, 103983.

- Zhou, D., Z. Gan, X. Shi, A. Patwari, E. Rush, C.-L. Bonzel, V. A. Panickan, C. Hong, Y.-L. Ho, T. Cai, et al. (2022). Multiview incomplete knowledge graph integration with application to cross-institutional ehr data harmonization. *Journal of Biomedical Informatics* 133, 104147.
- Zhou, D., H. Tong, L. Wang, et al. (2026). Representation learning to advance multi-institutional studies with electronic health record data from US and France. *Nature Communications*.
- Zhou, G., A. Cichocki, Y. Zhang, and D. P. Mandic (2015). Group component analysis for multiblock data: Common and individual feature extraction. *IEEE Transactions on Neural Networks and Learning Systems* 27(11), 2426–2439.